The EMBO Journal vol.14 no.7 pp.1532–1541, 1995

# The solution structure of the RING finger domain from the acute promyelocytic leukaemia proto-oncoprotein PML

**Katherine L.B.Borden[1], Michael N.Boddy[2], John Lally[2], Nicola J.O'Reilly[3], Stephen Martin[4], Kathy Howe[5], Ellen Solomon[5] and Paul S.Freemont[2,6]**

[1]Laboratory of Molecular Structure, [4]Division of Physical Biochemistry, National Institute for Medical Research, The Ridgeway, Mill Hill, London NW7 1AA and [2]Protein Structure Laboratory, [3]Peptide Synthesis Laboratory, [5]Somatic Cell Genetics Laboratory, ICRF, 44 Lincoln's Inn Fields, London WC2A 3PX, UK
[1]Present address: Protein Structure Laboratory, ICRF, London WC2A 3PX, UK

[6]Corresponding author

Communicated by E.Solomon

**Acute promyelocytic leukaemia (APL) has been ascribed to a chromosomal translocation event which results in a fusion protein comprising the PML protein and the retinoic acid receptor α. PML is normally a component of a nuclear multiprotein complex (termed ND10, Kr bodies, nuclear bodies, PML oncogenic domains or PODs) which is disrupted in the APL disease state. PML contains a number of characterized motifs including a $Zn^{2+}$ binding domain called the RING or $C_3HC_4$ finger. Here we describe the solution structure of the PML RING finger as solved by $^1H$ NMR methods at physiological pH with r.m.s. deviations for backbone atoms of 0.88 and 1.39 Å for all atoms. Additional biophysical studies including CD and optical spectroscopy, show that the PML RING finger requires $Zn^{2+}$ for autonomous folding and that cysteines are used in metal ligation. A comparison of the structure with the previously solved equine herpes virus IE110 RING finger, shows significant differences suggesting that the RING motif is structurally diverse. The role of the RING domain in PML nuclear body formation was tested *in vivo*, by using site-directed mutagenesis and immunofluorescence on transiently transfected NIH 3T3 cells. Independently mutating two pairs of cysteines in each of the $Zn^{2+}$ binding sites prevents PML nuclear body formation, suggesting that a fully folded RING domain is necessary for this process. These results suggest that the PML RING domain is probably involved in protein–protein interactions, a feature which may be common to other RING finger domains.**

*Keywords*: NMR/promyelocytic leukaemia/protein structure/RING finger

## Introduction

The human *pml* gene is associated with APL, which arises due to a block in the normal differentiation of promyelocytes (for review see Grignani *et al.*, 1994). In APL cells, *pml* is fused with retinoic acid receptor alpha (*rara*) following a reciprocal chromosomal translocation, t(15;17)(q22,q21) (Goddard *et al.*, 1991; Kakizuka *et al.*, 1991; de Thé *et al.*, 1991; Kastner *et al.*, 1992). *pml* is expressed apparently ubiquitously, transcripts being visible on Northern blots of all cell lines and tissues tested so far (Goddard *et al.*, 1991; Fagioli *et al.*, 1992). Recently, the PML protein has been shown to be part of nuclear multiprotein complexes known as ND10, nuclear bodies, PML oncogenic domains or PODs, Kr bodies, which are distinct from snRNPs and nucleoli (Ascoli and Maul, 1991; Xie *et al.*, 1993; Dyck *et al.*, 1994; Koken *et al.*, 1994; Weis *et al.*, 1994). Whilst the function of PML nuclear bodies is at present unknown, in leukaemic cells expressing the PML–RARA fusion protein, the distribution and size of these nuclear bodies is altered and they appear to become disrupted (Dyck *et al.*, 1994; Koken *et al.*, 1994; Weis *et al.*, 1994). Interestingly, treatment of these cells with retinoic acid reverses these changes and leads to the reformation of a normal PML nuclear body staining pattern (Dyck *et al.*, 1994; Koken *et al.*, 1994; Weis *et al.*, 1994). It has been shown by a number of groups that the PML–RARA fusion protein can bind to normal PML (Dyck *et al.*, 1994; Weis *et al.*, 1994) as well as RXR forming multiple heterodimers (Grigani *et al.*, 1993; Perez *et al.*, 1993). Recently, PML but not PML–RARA has been shown to be a growth suppressor in a variety of assay systems (Mu *et al.*, 1994) which has led to the suggestion that sequestration of normal PML would affect the growth suppressor activity of PML and sequestration of RXR the induction of differentiation (Mu *et al.*, 1994). It is now proposed that both molecular events are necessary for leukaemogenesis of APL (Mu *et al.*, 1994).

The *pml* coding sequence contains a number of novel motifs including three cysteine-rich metal binding domains and a predicted α-helical coiled-coil domain (e.g. see Goddard *et al.*, 1991; Reddy *et al.*, 1992). The first cysteine-rich region, the RING motif, defines a new family of proteins ubiquitously expressed in organisms ranging from plants to viruses, all of which have putative functions involving some aspect of transcriptional regulation (Freemont *et al.*, 1991; Freemont, 1993). Recently, a RING finger domain has been identified in the breast cancer susceptibility gene *BRCA1*, with one of the identified predisposing mutations resulting in a deletion of the RING finger (Futreal *et al.*, 1994; Miki *et al.*, 1994). Within the RING finger family, a second cysteine-rich motif has been identified called the B-box (Reddy and Etkin, 1991; Reddy *et al.*, 1992; Freemont, 1993). All B-box family members possess a RING finger and either one or two B-box motifs followed closely (five to eight amino acids) by a predicted α-helical coiled-coil dimerization domain forming a tripartite motif (Kastner *et al.*, 1992; Reddy *et al.*, 1992)

A

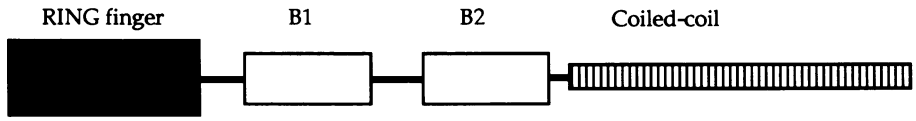


B

```
                    1         10          20         30                  40         50
PML   (49-104)      EEEFQFLRCQQCQAEAKCP  KLLPCLHTLCSGCLE          ASGMQCPICQAPWPLGADTPAL
T18   (59-158)     SRLNLLDTCAVCHQNIQSRVPKLLPCLHSFCQRCLP(37)PFATQVGVIRCPVCSQECAERHIIDNF
RFP   (8-57)       ECLQQETTCPVCLQYFAEP  MMLDCGHNICCACLA    RCWGTAETNVSCPQCRETFPQRHMRPNR
BRCA1 (16-76)      NAMQKILECPICLELIKEP  VSTKCDHIFCKFCML    KLLNQKKGPSQCPLCKNDITKRSLQEST

IEEHV (1-63)        MATVAERCPICLEDPSNYS MALPCLHAFCYVCIT      RWIRQNPTCPLCKVPVESVVHTIES
RING1 (11-71)      RSLHSELMCPICLDMLKNTM TTKECLHRFCSDCIV     TALRSGNKECPTCRKKLVSKRSLRPD
                          * *              * * * *                 * *
```

**Fig. 1.** (**A**) The tripartite motif for PML. B1 and B2 refer to the B-boxes and the coiled-coil to the predicted α-helical coiled-coil domain. (**B**) Sequence alignment of the human proto-oncogenic RING proteins, PML, T18 , RFP and BRCA1 (see text). The $Zn^{2+}$ ligands are shown in bold and are labelled with*. The top numbering refers to the PML RING peptide and the bracketed numbers to the whole protein sequences. The sequence of RING1 (Lovering *et al.*, 1993) and IEEHV (Barlow *et al.*, 1994) are shown for comparison.

(Figure 1A). The B-box family includes PML (Goddard *et al.*, 1991; Kakizuka *et al.*, 1991; de Thé *et al.*, 1991; Kastner *et al.*, 1992), the ret finger protein (RFP; Takahashi *et al.*, 1988 ) and T18 (Miki *et al.*, 1991; Kastner *et al.*, 1992) (Figure 1B), all of which are oncogenic in humans and mice when found as translocations that include the entire tripartite motif recombined with other genes. The occurrence of the RING finger in a number of human proto-oncoproteins including the breast cancer susceptibility gene product suggests an important and perhaps fundamental cellular role for the RING motif.

In order to understand at the molecular level the function of the RING motif as found in the human proto-oncoprotein PML and its role, if any, in APL, we have determined the solution structure of the PML RING finger domain. The PML RING structure represents the first structure of a eukaryotic RING domain and a comparison with the only other RING motif of known structure (equine herpes virus IE110 protein, IEEHV; Barlow *et al.*, 1994), shows that the RING motif is structurally diverse. We also show that a structured PML RING domain is necessary for PML nuclear body formation *in vivo*, a process which is disrupted in the APL disease state. These data suggest that the PML RING finger is involved in making protein–protein interactions, a molecular function which may be common to other RING finger domains.

## Results and discussion

### *The PML RING finger forms an autonomously folded domain in the presence of $Zn^{2+}$*

A 56 residue peptide corresponding to the PML RING finger domain was obtained using standard synthetic methods and subsequently purified to homogeneity. The boundaries of the PML RING finger domain were chosen on the basis of sequence alignments of the RING finger family (Freemont, 1993). To investigate the nature of the divalent metal ligation of the PML RING domain, we initially used optical spectroscopy to monitor absorbance changes of the PML peptide upon cobalt binding (Figure 2A). The cobalt titration showed absorbance maxima at $\lambda$ = 307/340–350 nm supporting cysteine ligation, and maxima at $\lambda$ = 605/650–690 nm suggesting tetrahedral coordination (Berg and Merkle, 1989). When a solution of the PML RING peptide in an excess of cobalt was titrated with $Zn^{2+}$, the characteristic cobalt spectra diminished indicating that $Zn^{2+}$ can replace the cobalt preferentially.

To characterize further the metal binding properties of the PML RING domain, small aliquots of $Zn^{2+}$ solutions were added to the peptide while using $^1H$ NMR to monitor changes in the spectral features which occurred upon $Zn^{2+}$ ligation (Figure 2B). These features included the appearance of resonances upfield of the methyl group indicative of the formation of tertiary structure and also the appearance of peaks downfield of the HOD resonance indicative of anti-parallel β-sheet formation. The amide protons were only protected against exchange with bulk solvent in the presence of $Zn^{2+}$ (Figure 2B). These data show that the PML RING domain is only structured in the presence of $Zn^{2+}$, which upon binding forms some β-strand structures. Furthermore, only one set of cross-peaks was observed for the PML RING peptide in subsequent 2D experiments, suggesting that the domain exists as a monomer in solution. The far-UV CD spectrum of the PML RING peptide in aqueous solution shows only low intensity above 210 nm, suggesting a small amount of regular secondary structure (data not shown). The addition of 200 μM $ZnCl_2$ however, causes a small reduction in intensity at 200–205 nm and a small increase in intensity at longer wavelengths. These changes are reversible by the addition of excess EDTA indicating that any structural

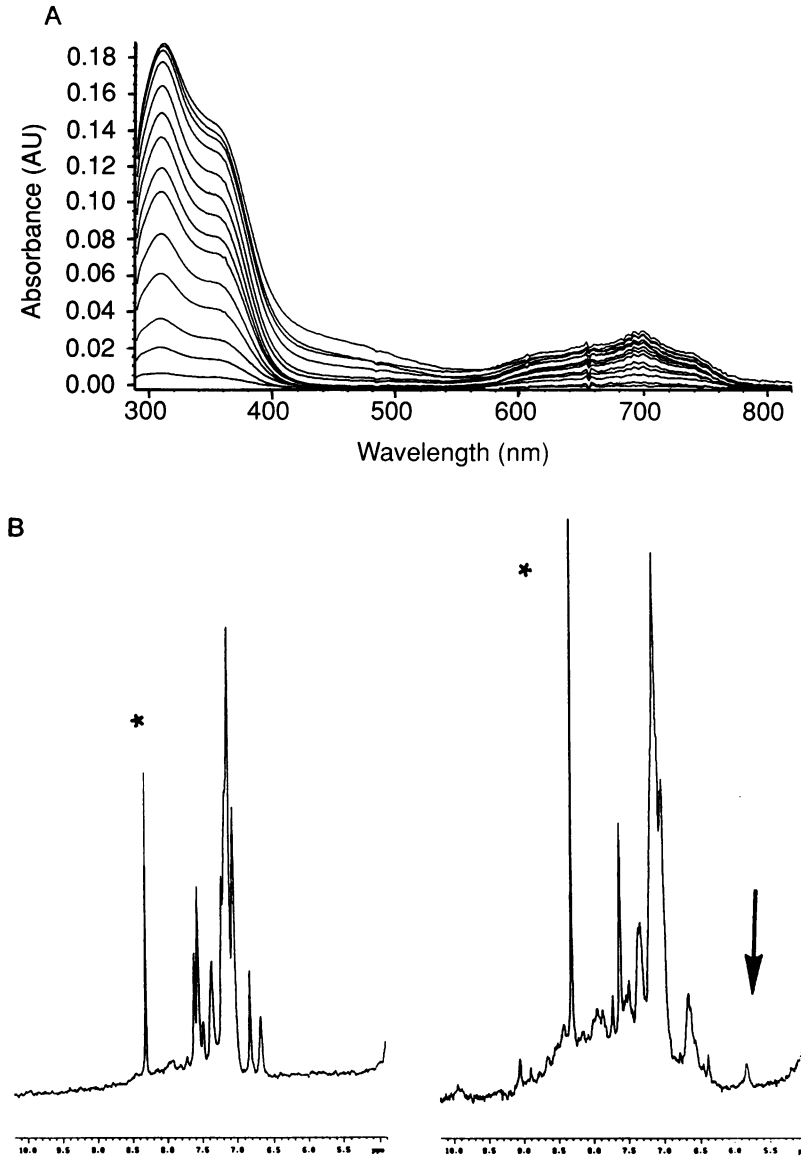


**Fig. 2.** Characterization of the divalent metal binding properties of the PML RING peptide. (**A**) Cobalt titration of the PML RING peptide. The spectrum shown represents a single experiment using 54 μM peptide. Cobalt was added in increments of 5 μM from 1 to 40 μM and then 10 μM from 40 to 100 μM. (**B**) One-dimensional $^1$H NMR spectra in water for PML RING finger domain before the addition of $Zn^{2+}$ (left) and after the addition of $Zn^{2+}$ (right) showing the appearance of amide protons after $Zn^{2+}$ addition. The arrow indicates one of the alpha carbon protons which is shifted downfield of the HOD resonance. * indicates a contaminant.

changes are $Zn^{2+}$ dependent. The observed changes in the CD spectra upon $Zn^{2+}$ addition are consistent with the PML RING peptide forming a small amount of β-strand structure (~15%) with little α-helix.

### *The NMR structure determination*

The three dimensional structure of the PML RING domain was determined using standard two dimensional NMR techniques (see Materials and methods). A summary of the NOE connectivities is given in Figure 3A and the number of restraints for each residue in Figure 3B. An initial set of structures was generated without reference to metal ligation in order to determine the residues involved in $Zn^{2+}$ binding. These structures indicated that residues Cys9, Cys 12, Cys29 and Cys32 form a single $Zn^{2+}$ binding site whilst Cys24, His26, Cys40 and Cys43 form another. These sites were defined partially by the individual NOEs observed between residues implicated in $Zn^{2+}$ ligation (see Figure 3A). For example, NOEs were observed between Cys9 and Cys29, Cys24 and Cys40, His26 ring and Cys43, Cys40 plus several other NOEs between residues adjacent to the $Zn^{2+}$ ligands (Figure 3A). At this stage the r.m.s. deviation for 44 structures (residues 4–51) for backbone atoms was 1.1 Å and 1.6 Å for all atoms. Subsequently, the $Zn^{2+}$ atoms were included in the calculations using additional constraints as described by Neuhaus *et al.* (1992), to define the tetrahedral geometry of the $Zn^{2+}$ binding site as indicated by our cobalt binding data (see Figure 2A). The delta nitrogen of the H26 ring was used in ligation instead of the more usual epsilon nitrogen. The epsilon nitrogen could be ruled out on the basis of NOEs observed from the HD2 and HE1 protons of the His ring. The structure of the IEEHV RING domain also shows a similar $Zn^{2+}$ ligation arrangement including

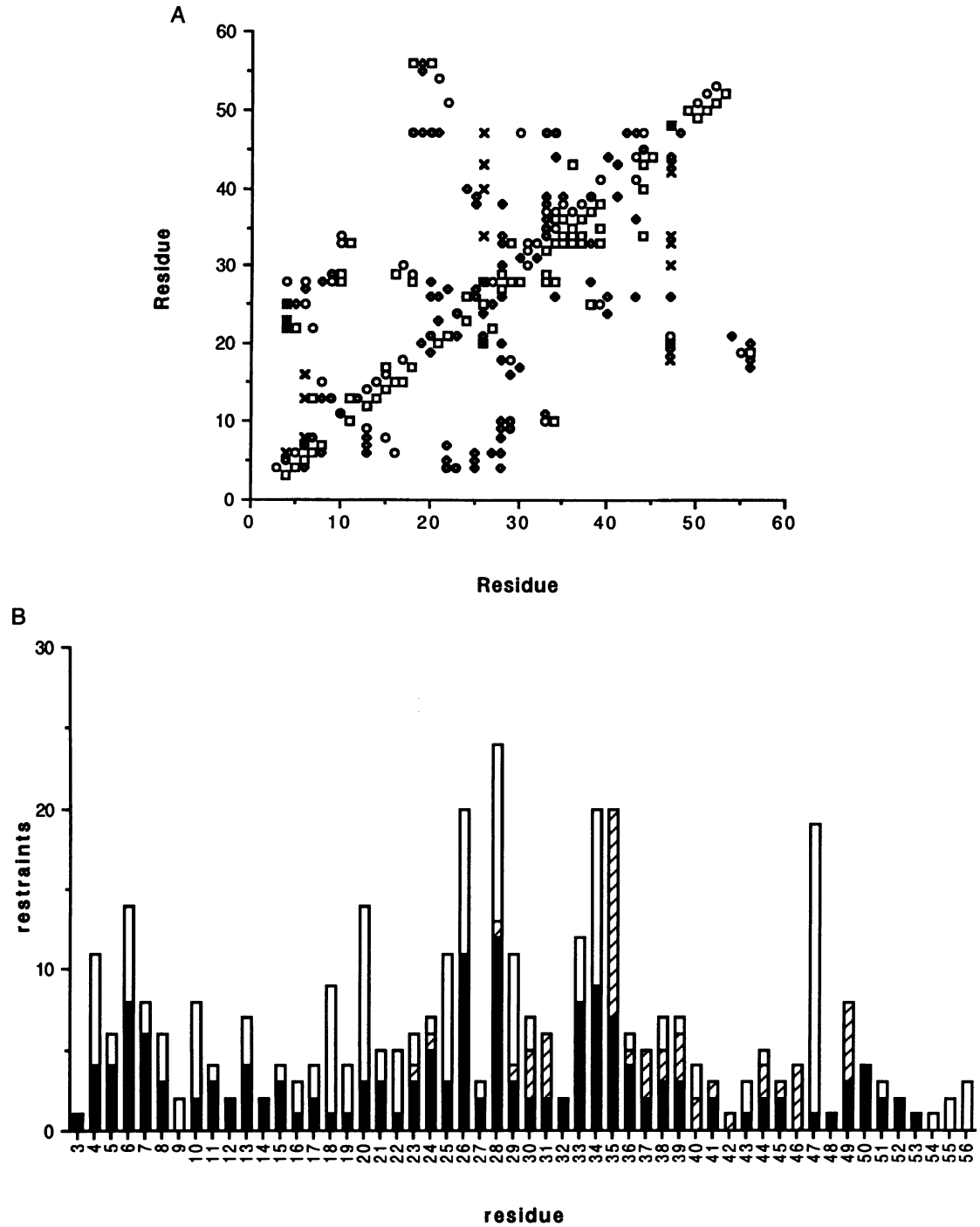


**Fig. 3.** NMR data used in the PML structure calculations. (**A**) A distance map summarizing the NOEs observed for the PML RING domain. Reading the residue number from the x-axis indicates the type of proton observed. The symbols are as follows: ○ amide proton, ◇ alpha carbon proton, □ side chain proton, × ring proton. (**B**) Distance restraints per residue are shown with long range (white), medium range (hatched) and short range (black).

the use of the delta nitrogen as a $Zn^{2+}$ ligand (Barlow *et al.*, 1994).

In total there were 197 unique non-redundant distances not including intra-residue distances (84 long, 31 medium, 82 short range) and 26 angle constraints (15 phi, 8 psi, $3\chi_1$). Two hydrogen bond constraints were included on the basis of slow exchanging amides. The criteria for slow exchanging amide protons was very stringent, with only those amide protons used which were still present after 48 h in $^2H_2O$. There were several slow exchanging amides but in most cases hydrogen bonding partners could not be unambiguously singled out. Of the 44 structures used in the refinement, 22 structures converged with NOE errors of <0.5 Å and angle violations of <10°. The remaining structures were similar to these but had minor distance or angle violations which were beyond the allowed cut-offs. An overall r.m.s. deviation for 22 structures for residues 4–51 was 0.88 Å for backbone and 1.39 Å for all atoms indicating that the number of constraints was sufficient to allow good convergence. An alpha carbon backbone

overlay for residues 4–56 is shown in Figure 4A. A similar overlay but with the side chains of Phe4, Phe6, Leu28 and Trp47 is shown in Figure 4B. The r.m.s. separation between the average structure prior to and after inclusion of $Zn^{2+}$ parameters was 0.59 Å for backbone and 0.77 Å for all atoms, demonstrating that the overall structure did not change significantly after inclusion of $Zn^{2+}$ in the structure calculations.

### *The PML RING finger structure*

The PML RING finger domain is nearly spherical in shape (~27 Å×24 Å×22 Å) and comprises four β-strand regions, a single turn of $3_{10}$ helix and a number of loops and turns (Figure 4C). The first three residues are not structured and lead into a β-strand (β1; residues 5–8) which continues into a loop forming part of $Zn^{2+}$ binding site I (residues 9–16). An extended region (residues 17 and 18) leads into a second β-strand (β2; residues 19–21) which continues into part of $Zn^{2+}$ binding site II (residues 22 and 25) and is followed by a third β-strand (β3; residues 26–28) antiparallel to β2. $Zn^{2+}$ binding site I is completed by a loop (residues 29–33) which leads into a helical turn (34–38) and then into the second part of $Zn^{2+}$ binding site II (residues 39–44). Residues 45–48 form one turn of $3_{10}$ helix with sequence Ala-Pro-Trp-Pro which lies perpendicular and across the central β-strands β2 and β3 (Figure 4C). A loop from 49 to 52 leads into a small, less well defined β-strand (β4; residues 53–56) at the C-terminus. The two $Zn^{2+}$ atoms are ligated by Cys9, 12, 29 and 32 and Cys24, His26 and Cys40,43 in a 'cross-brace' similar to that for the IEEHV RING domain (Barlow *et al.*, 1994). The PML RING structure is stabilized by a number of hydrophobic interactions. Leu28 is at the centre of the hydrophobic core packing with Phe6, Cys18, Leu25, Leu33, Met38. Phe4, Leu22 and Thr27 are also involved in hydrophobic packing. There is another mini hydrophobic core involving His26, Lys20 and Trp47. The amino group of the Lys20 is at the surface of the molecule although most of the side chain is buried.

### *Comparison of the PML and IEEHV RING finger structures*

In the context of the RING family, the IEEHV and PML RING fingers have a number of hydrophobic residues which are conserved and form the core of both structures, as is the 'cross-brace' $Zn^{2+}$ binding arrangement and the topology of the central β-strands. However, both RING finger domains have little sequence homology (15% identity) outside of the $Zn^{2+}$ binding residues (Figure 1), which is reflected in the observed structural differences between both domains. A three residue insertion in the IEEHV RING sequence forms part of a two-turn α-helix which is absent in the PML RING structure (Figure 5A), as observed in both the CD and NMR experiments (see above). There is also an insertion between positions 19 and 20 in IEEHV relative to PML which probably affects the conformation of $Zn^{2+}$ binding site II (Figure 1). Furthermore, the region corresponding to PML strand β1 is disordered in the IEEHV structure. It should be noted that the PML (pH 7.5) and IEEHV (pH 6.3) structures were determined at different pH values which may give rise to some structural differences. Interestingly, the two $Zn^{2+}$ atoms are ~14 Å apart in both structures presumably due to the conservation in residue spacing in the central portion of the RING motif and the unique 'cross-braced' $Zn^{2+}$ ligation system used to form the two $Zn^{2+}$ binding sites (Figure 5A). A r.m.s. separation of 4.5 Å on Cα atoms for residues 8–12 (7–11 in IEEHV), 22–33 (22–33 in IEEHV) and 40–43 (43–46 in IEEHV) can be obtained in a superposition of the PML and IEEHV RING structures (Figure 5A).

Interestingly, from the superposition some of the equivalent core hydrophobic residues overlap in space including Leu22/Leu21(IEEHV) and Leu28/Phe28(IEEHV), suggesting that despite the obvious structural rearrangements, the core of the domain is maintained. It also appears that some core hydrophobic residues, which are not equivalent in the sequence alignment, become equivalent in the three-dimensional structure alignment including Leu33/Trp36 (IEEHV), Trp47/Ile33 (IEEHV) and Leu25/Leu45 (IEEHV). If only those residues from PML and IEEHV which form $Zn^{2+}$ binding site I are superposed, a r.m.s. separation of 1.93 Å on C-α atoms for residues 8–18 (7–17 in IEEHV) and 27–33 (27–33 in IEEHV) can be obtained (Figure 5B). It appears that most of the structural changes occur between the central β-strands and the last pair of $Zn^{2+}$ ligands within both RING domains, resulting in a different relative conformation for $Zn^{2+}$ binding site II. These structural alterations are consistent with this region being the most diverse in terms of primary sequence and length among RING family members and may infer different functions and/or specificity of RING finger domains within different proteins (Freemont, 1993). In summary, it appears that the RING finger motif can adopt significantly varying three-dimensional structures whilst maintaining some structural conservation including the overall topology of the central β-strands, the cross-braced $Zn^{2+}$ binding system and the packing of conserved residues which form the hydrophobic core. This would suggest that the RING finger motif forms a convenient scaffold which can be structurally varied to reflect a diversity in molecular function.

### *A mutated PML RING finger does not form PML nuclear bodies in vivo*

In the PML RING structure, $Zn^{2+}$ tethers the different secondary structural elements together as well as the two loop regions at each end of the molecule forming a scaffold (Figure 4C). In order to test the *in vivo* functional importance of $Zn^{2+}$ ligation in the PML RING finger domain, mutants in RING within whole PML (~69 kDa PML isoform) were prepared that would affect $Zn^{2+}$ binding at either site one (Cys57,60ΔAla; corresponding to Cys9,12 in the peptide numbering) or site two (Cys88, 91ΔAla; corresponding to Cys40,43 in the peptide numbering). These mutants were transiently transfected into NIH 3T3 cells and visualized by indirect immunofluorescence using a polyclonal anti-PML antibody. Prior to use the PML antibody was purified against a peptide corresponding to residues 228–267 in the predicted coiled-coil region of PML which has low homology to the equivalent region of the mouse protein (A.Goddard and E.Solomon, unpublished observations). It is interesting to note that the purified antibody does not cross-react with endogenous mouse PML unlike the crude antiserum. Transfected wild type PML results in a punctate nuclear

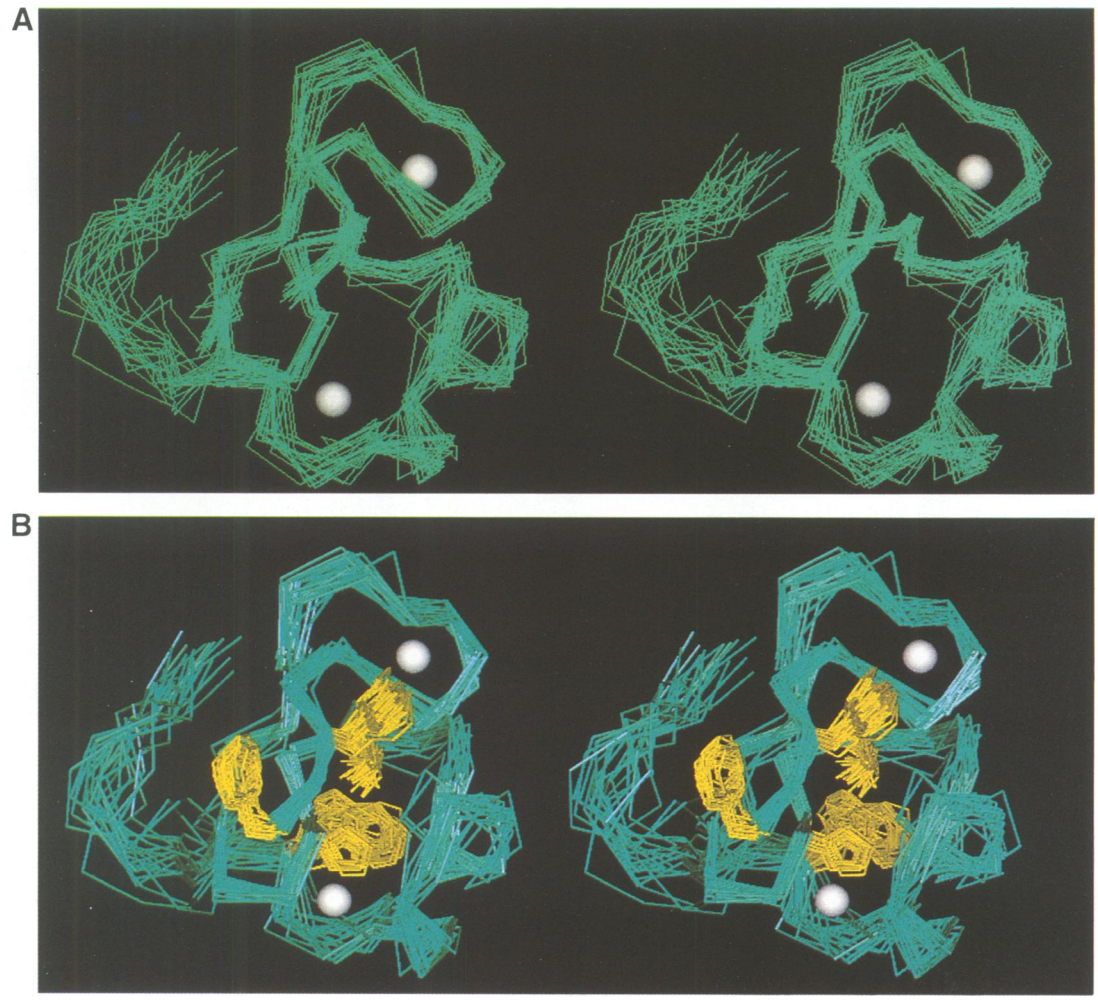


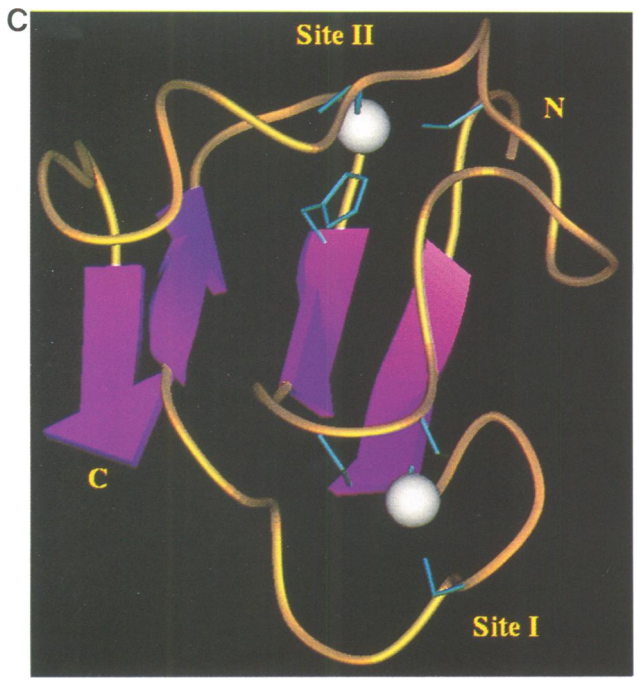


**Fig. 4.** The PML RING finger structure. (**A**) α-Carbon overlay of 22 PML RING domain structures. The three N-terminal residues are disordered and are not shown. The average position of the two $Zn^{2+}$ atoms are represented as white spheres. The average NOE energy for the 22 structures was 53 ± 15 kcal/mol and the overall energy was 458 ± 42 kcal/mol. Deviations from idealized covalent geometry were bonds 0.0059 ± 0.0004 Å, angles 1.24 ± 0.04° and impropers of 0.74 ± .05°. (**B**) Same overlay as in (A) but with side chains Phe4, Phe6, Leu28 and Trp47 shown in yellow. (**C**) Topology of the PML RING finger domain. The four β-strand regions are shown as arrows (magenta). The cysteines and histidine side chains which form the two $Zn^{2+}$ binding sites (I and II) are shown in blue. The two $Zn^{2+}$ atoms are represented as white spheres and the N- and C-termini are labelled. Images were made using the program PREPI (S.Islam and M.Sternberg, ICRF).

pattern characteristic of endogenous PML protein (Figure 6A). Transfection of both mutant PML proteins however, showed a diffuse nuclear staining pattern remaining excluded from nucleoli (Figure 6B,C). These results are consistent with the previous observation that a double mutation Gln59ΔGlu, Cys60ΔLeu can disrupt the speckled PML nuclear staining pattern in transiently transfected Cos-1 cells (Kastner *et al.*, 1992).

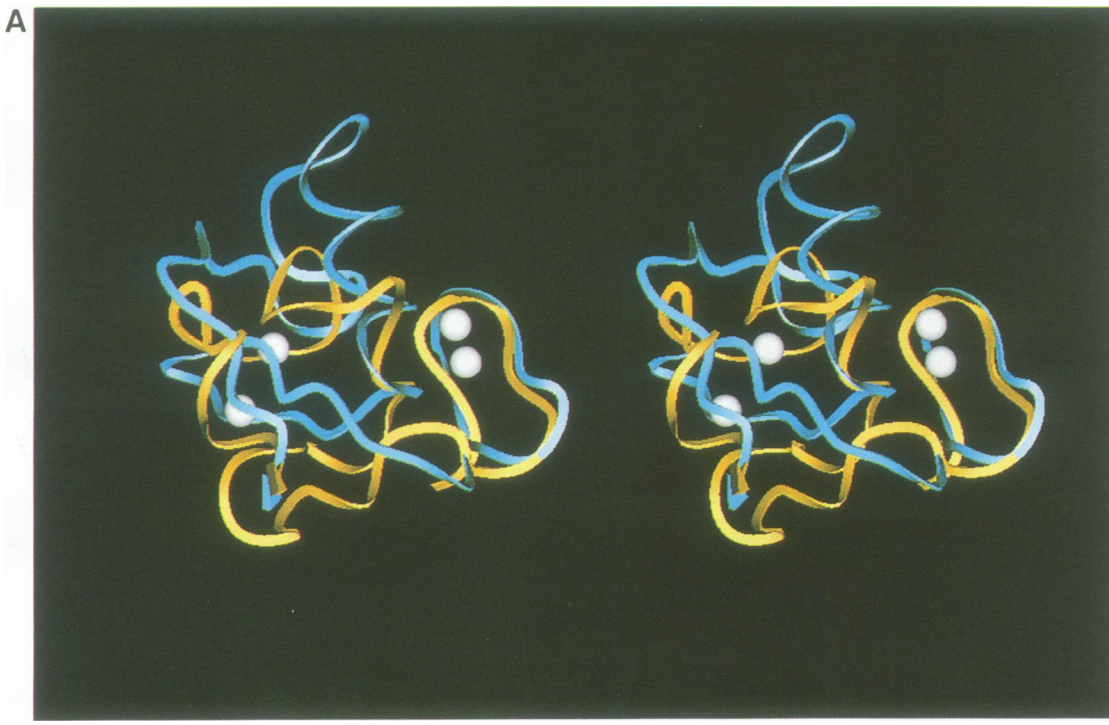


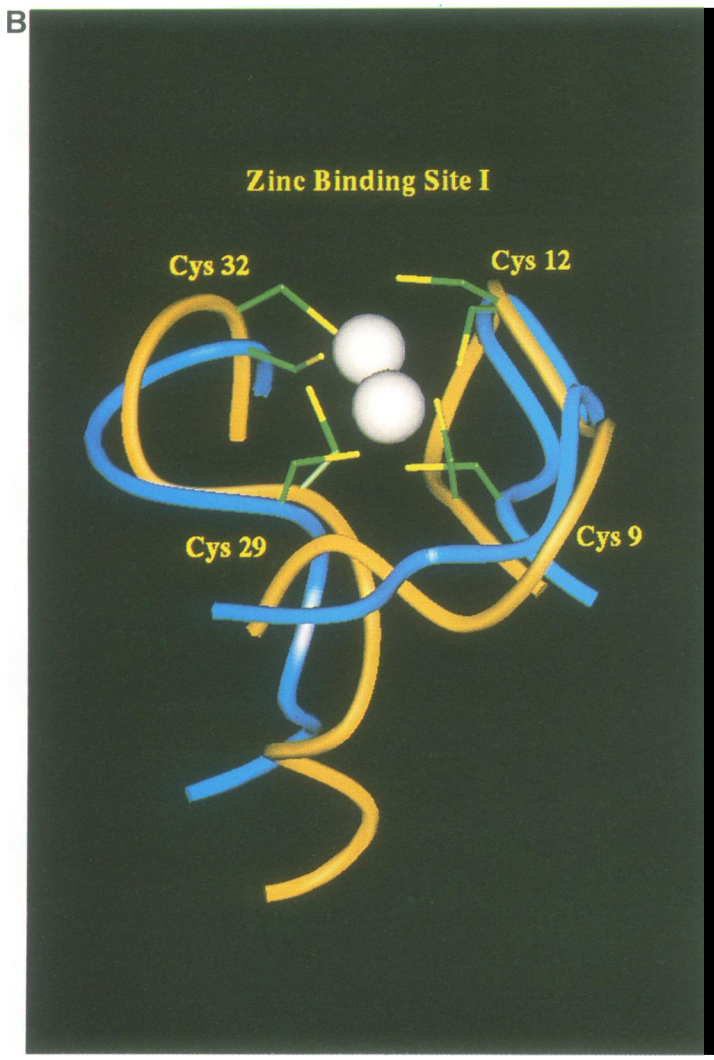


**Fig. 5.** Comparison of the PML and IEEHV RING structures. (**A**) Stereo view of the superposition of PML (residues 7–48; gold) and IEEHV (residues 7–56; blue) using only PML residues 8–12, 22–33 and 40–43 to calculate the superposition matrix (see text). The $Zn^{2+}$ atoms are represented as white spheres and arrows indicate the C-terminal end. (**B**) Superposition of $Zn^{2+}$ binding site I for PML (residues 8–18; 24–33) and IEEHV (residues 7–17; 25–33). The $Zn^{2+}$ atoms are represented as white spheres and the cysteine ligands are labelled. The numbering corresponds to the PML peptide (see Figure 1B). Images were made using the program PREPI (S.Islam and M.Sternberg, ICRF).

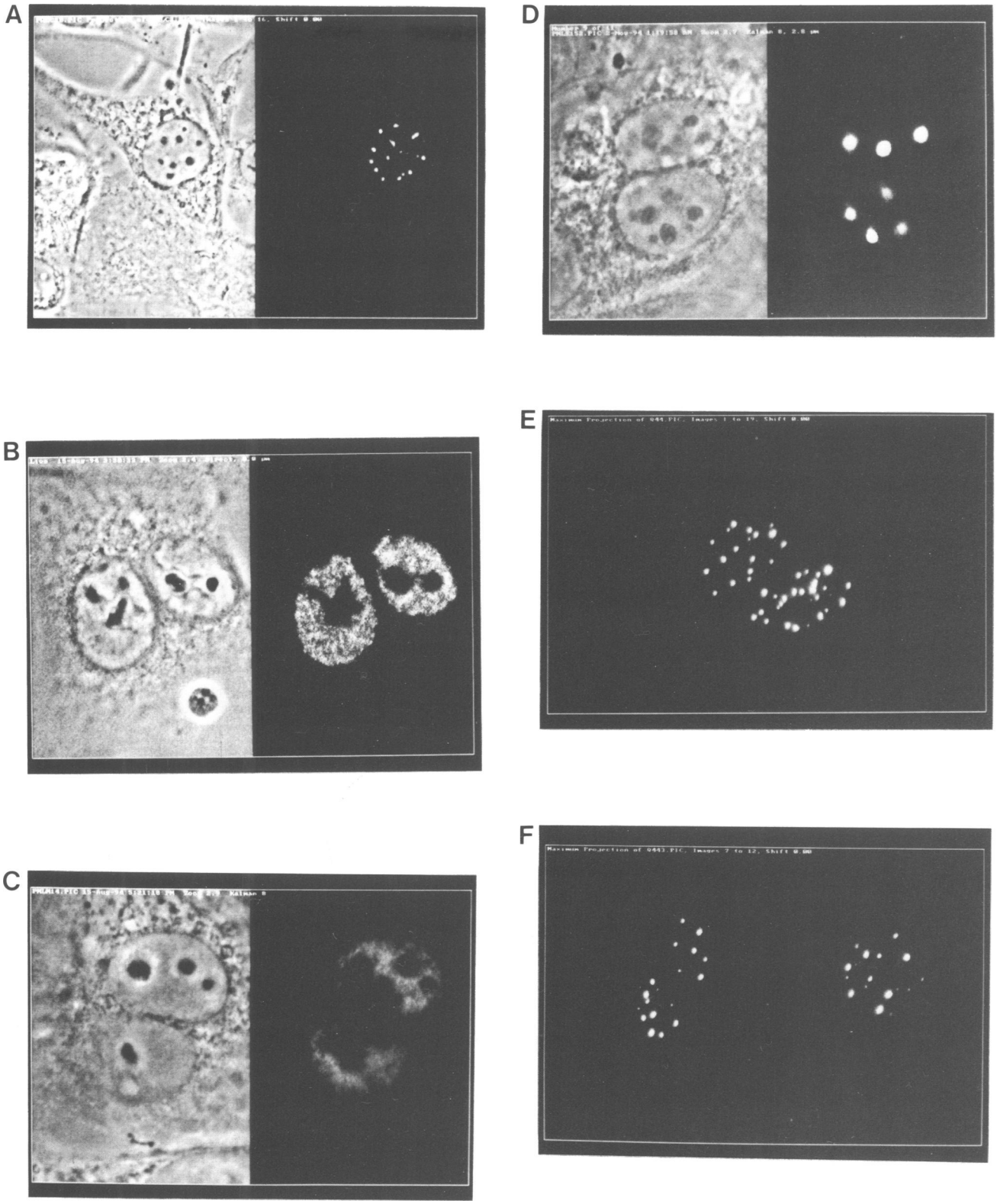


**Fig. 6.** Analysis of PML RING finger mutants by transient transfection and indirect immunofluorescence. (A–D) show phase (left) and fluorescence (right; E and F only) images of NIH 3T3 cells transiently transfected with; (**A**) wild type PML, (**B**) PML (Cys57,60ΔAla); (**C**) PML (Cys88,91ΔAla); (**D**) PML (Glu15ΔArg); (**E**) PML (Gln39ΔGlu); (**F**) PML (Gln44ΔGlu).

The inability of the mutant PML proteins to form nuclear bodies suggests that a correctly folded RING domain is essential to this process as mutations of cysteines at either $Zn^{2+}$ binding site would interfere with the folding of the domain. Furthermore, CD and 1D NMR studies show that $Zn^{2+}$ is necessary for the PML RING finger domain to fold *in vitro* (see above). It is possible that these double-point mutations could disrupt the overall fold of the entire PML protein. However, PML is a large protein (minimum 560 residues) and comprises a number

of discrete modular domains (see Grignani *et al.*, 1994). Furthermore, it has been shown in other systems that such modular proteins can consist of autonomously folded units independent of each other (for review see Campbell and Spitzfaden, 1994). However, the possibility that disruption of the PML RING affects the overall structure of PML cannot at this stage be excluded. It is also possible that other domains within the PML protein are required for PML nuclear body formation, but our results clearly show that a structured RING domain is necessary and may be involved in promoting protein–protein interactions.

To analyse further the role of the PML RING finger in nuclear body formation, a number of surface residue mutations were made based on the PML RING structure. The residues chosen are not involved in forming core interactions and would therefore be unlikely to affect the integrity of the RING domain. The following mutations: Gln39ΔGlu; Gln44ΔGlu; Gln10,11,13ΔGlu and Arg8ΔSer; Glu15ΔArg; Arg8ΔGlu were prepared and transiently transfected into NIH 3T3 cells and visualized by indirect immunofluorescence (Figure 6). The most striking mutant is Glu15ΔArg where a consistently small number of abnormally large PML nuclear bodies is observed in a population of transfected cells (Figure 6D) as compared with wild type (Figure 6A). The quadruple mutation generally resulted in increased numbers of small PML nuclear bodies relative to wild type (data not shown). The Gln39ΔGlu and Gln44ΔGlu mutants however, did not appear to affect PML nuclear body formation relative to wild type (Figure 6E and F respectively, compared with Figure 6A) as did the Arg8ΔGlu mutant (data not shown), although they may have had other effects which are not detected using this assay system. These data suggest that the surface area most important to PML nuclear body formation is the region around Glu15 and the first half of zinc binding site I, which are spatially near to each other. Interestingly, Gln39 and Gln44, which are at the other end of the molecule, appear to have no effect. Electrostatic surface potential calculations indicate that the PML RING domain is nearly uniformly positive with only a few isolated negative potential patches, one of which is Glu15 (P.Bates, unpublished observations). These results strongly suggest that there is a surface charge component to PML nuclear body formation. In conclusion, the PML RING structure now provides the basis for in depth site-directed mutagenesis studies to determine in more detail the molecular role of the RING finger domain in PML function.

## Materials and methods

### *Peptide synthesis and purification*

A peptide comprising residues 27 to 82 of PML was synthesized on a Model 431A Applied Biosystems Solid Phase Synthesizer and purified as described previously (Borden *et al.*, 1993). The yield of the 56mer was ~20%. A few micrograms of the pure PML peptide (peak fraction from HPLC separation) were analysed by Matrix-Assisted Laser Desorption mass spectrometry (Karas and Hillenkamp, 1988). A single species was observed with an experimental molecular weight [$M(H^+)$] of 6109.4 Daltons which is in excellent agreement with the calculated mass of 6109.1 Daltons for the fully reduced form of the peptide. The concentration of PML RING peptide was measured optically using a calculated extinction coefficient of 0.934 for 1 mg/ml solution measured at 280 nm. The sample was purified in the presence of ethanedithiol and in general, subsequent experiments had trace amounts of ethanedithiol present.

### *Optical spectroscopy, circular dichroism and $^1H$ NMR experiments*

Cobalt binding studies, CD and 1D $^1H$ NMR methods were used to determine the metal binding properties of the PML peptide. The cobalt binding reactions were monitored on an HP 8452 diode array spectrophotometer using a 1 cm path length at room temperature. The spectra were corrected by subtracting the contribution from the peptide and buffer alone. Typically, a solution (1 ml) containing 40–50 μM of PML RING peptide (10 mM Tris–HCl pH 7.5) was titrated with solutions of $CoCl_2$. The peptide was also titrated against solutions of $ZnCl_2$ in the presence of 80–100 μM $CoCl_2$. CD spectra were recorded on a Jasco J-600 spectropolarimeter at room temperature in 20 mM Tris at pH 7.5. Far-UV CD spectra (200–260 nm) were measured using 2 mm fused silica cuvettes and PML peptide concentrations of ~40 μg/ml. Near-UV CD spectra (255–340 nm) were measured using 10 mm fused silica cuvettes with PML peptide concentrations of ~400 μg/ml. Multiple scans were averaged (≥8 for near-UV and ≥4 for far-UV), and baselines subtracted. For 1D $^1H$ NMR measurements, ~5 mg of the PML peptide was dissolved in 10 mM sodium phosphate and 100 mM KCl at pH 7.5* (uncorrected for isotope effects) in 0.5 ml of either $^1H_2O$ or $^2H_2O$. The proton chemical shifts were referenced to 0.1 mM internal sodium tetradimethyl-2,2,3,3-tetra-deutero-4,4-dimethyl-4-silapentanoic acid. All NMR experiments were carried out at 30°C. Argon gas was bubbled through the solution to decrease problems with precipitation. The final sample concentrations were between 1 and 2 mM. The peptide was not soluble at higher concentrations. $^1H_2O$ samples contained 10% $^2H_2O$ to provide a lock signal. When further additions of $Zn^{2+}$ caused no further shifting of the peaks the peptide was considered to be fully saturated with metal ion.

### *NMR experiments*

TOCSY, DQF-COSY, NOESY and ROESY in $^2H_2O$ and TOCSY and NOESY experiments in $^1H_2O$ were carried out in order to determine the three-dimensional solution structure of the PML RING domain. 1D and 2D $^1H$ NMR experiments were collected at 11.7 and 14.1 T on Varian Unity spectrometers. Phase sensitive data were collected using the method of States *et al.* (1982). A $^1H$ TOCSY experiment with a 50 ms mixing time using MLEV17 (Bax and Davis, 1985) to produce the isotropic mixing was recorded both in $^1H_2O$ and $^2H_2O$. The spin-lock field strength was 8.9 kHz. The acquisition time was 500 ms in $t_2$ and 42 ms in $t_1$, with a 2.6 s recycle delay. A phase-sensitive NOESY experiment in $^2H_2O$ with 260 ms mixing time was recorded. A total of 400 increments of 4096 points were collected with a 2.4 s recycle delay. The acquisition time was 256 ms in $t_2$ and 40 ms in $t_1$. A series of NOESY experiments were also collected in $^1H_2O$. The intense water signal was suppressed using presaturation. A 180° pulse was applied in the middle of the mixing time to maintain suppression of the $^1H_2O$ signal. The NOESY experiment was collected with mixing times from 170 to 290 ms where 260 ms was found to be the optimal mixing time. A total of 400 increments with 4096 or 8192 data points were collected. The acquisition time was 256–512 ms in $t_2$ and 40 ms in $t_1$. One NOESY experiment ($t_m$–290ms) was collected with a pre-TOCSY in order to recover bleached alpha protons (Otting and Wüthrich, 1987). In this case the experiment was collected with a 25 ms pre-TOCSY mixing time and a spin-lock field strength of 7.7 kHz using MLEV17 to produce the isotropic mixing. ROESY and DQF-COSY experiments were also carried out in $^2H_2O$. The ROESY experiment was collected with a 130 ms mixing time and a spin-lock field strength of 3.3 kHz according to the methods of Bothner-By *et al.* (1984) and Bauer *et al.* (1990). Four hundred increments with 4096 data points and 2.5 s recycle delay were used. For the DQF-COSY experiment, 600 increments were collected in $t_1$ with 4096 data points. Free induction decays were zero-filled once or twice times in each dimension and apodized with a Gaussian function prior to Fourier transformation.

### *Generation of restraints*

Standard sequential two-dimensional $^1H$ NMR methods were used to assign 86% of the amide proton resonances and 96% of the side-chain resonances. Pseudoatom corrections were used as described by Wüthrich (1986). A comprehensive list of NOE connectivities was compiled and divided into categories based on the intensity of the cross-peaks and then ascribed upper distance limits. Phi, Psi and Chi1 angles were also extracted from the data. Phi angles were obtained from measuring the value of the $^3J_{\alpha N}$ coupling constants in high digital resolution TOCSY experiments (Searle, 1993). Psi angles were calculated using the program PROPHET (A.N.Lane, unpublished) which uses the distances between the $\alpha H_i$ and $NH_{i+1}$ and $\beta H_1$ to $NH_{i+1}$, and $^3J_{\alpha N}$. Chi1 values were

obtained using the method of Wagner *et al.* (1987) where the distances between αH and $\beta_1$H and αH and $\beta_2$H were extracted from ROESY experiments in order to avoid the problem of spin-diffusion. Values for $J\alpha\beta_1$,$J\alpha\beta_2$, $dN\beta_1$ and $dN\beta_2$ were also used.

### Structure calculations

Distance and angle constraints were used as input into XPLOR versus 3.1 (Nilges *et al.*, 1988; Brünger, 1992). The distance geometry embedding procedure was carried out followed by simulated annealing, slow cooling and 1000 steps of Powell energy minimization. Fifty structures were calculated using the XPLOR protocol with the following changes: molecules were heated to 1000 K, and were then allowed to cool slowly to 100 K in 4000 steps. From the 50 structures calculated, 44 converged into properly folded peptides while six formed the pseudo mirror image. The $Zn^{2+}$ atoms were then included in the XPLOR calculations with additional constraints as previously described (Neuhaus *et al.*, 1992) to maintain the tetrahedral bonding geometry of the sites and the correct bond lengths. These structures were refined and energy minimized in XPLOR as described above.

### Plasmids and site-directed mutagenesis

Mutagenesis was performed on the PML RING finger using a PCR 'stitching' method (Mullis *et al.*, 1986), producing an *Nco*I–*Avr*II fragment (15–300 bp). This *Nco*I–*Avr*II fragment, along with the remainder of the PML cDNA (*Avr*II–*Xho*I 300–1745 bp), was cloned into a mammalian expression vector carrying the MLV enhancer (Dalton and Treisman, 1992). Constructs were sequenced to confirm the mutations.

### PML antibody

PML (15–1745 bp) was bacterially expressed (pET-15b expression system, Novagen) according to the supplier's method. This material was used to raise a polyclonal antiserum that was affinity purified against a synthetic peptide corresponding to residues 228–267 of PML.

### Transfection and immunofluorescence

NIH 3T3 cells were transiently transfected using the DEAE–dextran shock method using 8 μg of each construct (Vaheri and Pagano, 1965) and after 40 h fixed at −20°C in MetOH for 10 min prior to immunofluorescence studies. Transfected PML protein was detected using neat affinity purified anti-PML polyclonal antiserum, that does not detect endogenous mouse PML, followed by an anti-rabbit FITC conjugated secondary antibody at 1:200 dilution (Dakopatts Ltd).

## Acknowledgements

We would like to thank Andrew Lane, Paul Barlow, Paul Bates, Mike Gradwell and Mike Sternberg for their comments and advice. This work is supported by the Imperial Cancer Research Fund, the Medical Research Council, UK and EEC Biotech Grant BIO2-CT93-0450 to E.F.

## References

Ascoli,C.A. and Maul,G.G. (1991) *J. Cell Biol.*, **112**, 785–795.
Barlow,P.N., Luisi,B., Milner,A., Elliott,M. and Everett,R. (1994) *J. Mol. Biol.*, **237**, 201–211.
Bauer,C.J., Frenkiel,T.A. and Lane,A.N. (1990) *J. Magn. Reson.*, **87**, 144–152.
Bax,A. and Davis,D.G. (1985) *J. Magn. Reson.*, **65**, 355–360.
Berg,J.M. and Merkle,D.L. (1989) *J. Am. Chem. Soc.*, **111**, 3759–3761.
Borden,K.L.B., Martin,S.R., O'Reilly,N.J., Lally,J.M., Reddy,B.A., Etkin,L.D. and Freemont,P.S. (1993) *FEBS Lett.*, **355**, 255–260.
Bothner-By,A.A., Stevens,R.L., Lee,J.T., Warren,C.D. and Jeonloz,R.W. (1984) *J. Am. Chem. Soc.*, **106**, 811–813.
Brünger,A.T. (1992) *XPLOR. A System for X-ray Crystallography and NMR*. Yale University Press, New Haven, CT.
Campbell,I.D. and Spitzfaden,C. (1994) *Structure*, **2**, 333–337.
Dalton,S. and Treisman,R. (1992) *Cell*, **68**, 597–612.
Dyck,J.A., Maul,G.G., Miller,W.H., Chen,J.D., Kakizuka,A. and Evans,R.M. (1994) *Cell*, **76**, 333–343.
Fagioli,M. *et al.* (1992) *Oncogene*, **7**, 1083–1091.
Freemont,P.S. (1993) *Ann. NY Acad. Sci.*, **684**, 174–192.
Freemont,P.S., Hanson,I.M. and Trowsdale,J. (1991) *Cell*, **64**, 483–484.
Futreal,P.A. *et al.* (1994) *Science*, **266**, 120–122.
Goddard,A.D., Borrow,J., Freemont,P.S. and Solomon,E. (1991) *Science*, **542**, 1371–1374.
Grignani,F. *et al.* (1994) *Blood*, **83**, 10–25.
Grignani,F. *et al.* (1994) *Cell*, **74**, 423–431.
Kakizuka,A., Miller,W.H., Umesono,K., Warrel,R.P.,Jr, Frankel,S.R., Murty,V.V.V.S., Dimetrovsky,E. and Evans,R. (1991) *Cell*, **66**, 663–674.
Karas,M. and Hillenkamp,F. (1988) *Anal. Chem.*, **60**, 2299–2301
Kastner,P. *et al.* (1992) *EMBO J.*, **11**, 629–642.
Koken,M.H.M. *et al.* (1994) *EMBO J.*, **13**, 1073–1083.
Lovering,R. *et al.* (1993) *Proc. Natl Acad. Sci. USA*, **90**, 2112–2116
Miki,T., Fleming,T.P., Crescenzi,M., Molloy,C., Blam,S., Reynolds,S. and Aaronson,S. (1991) *Proc. Natl Acad. Sci. USA*, **88**, 5167–5171.
Miki,Y. *et al.* (1994) *Science*, **266**, 66–71.
Mu,Z.-M., Chin,K.-V., Liu,J.-H., Lozano,G. and Chang,K.-S. (1994) *Mol. Cell. Biol.*, **14**, 6858–6867.
Mullis,K., Faloona,F., Scharf,S., Saiki,R., Horn,G. and Erlich,H. (1986) *Cold Spring Harbor Symp.*, **51**, 263–273.
Neuhaus,D., Nakaseko,Y., Schwabe,J.W.R. and Klug,A. (1992) *J. Mol. Biol.*, **228**, 637–651.
Nilges,M., Clore,G.M. and Gronenborn,A.M. (1988) *FEBS Lett.*, **229**, 317–324.
Otting,G. and Wüthrich,K. (1987) *J. Magn. Reson.*, **75**, 546–549.
Perez,A., Kastner,P., Sethi,S., Lutz,Y., Reibel,C. and Chambon,P. (1993) *EMBO J.*, **12**, 3171–3182.
Reddy,B.A. and Etkin,L.D. (1991) *Nucleic Acids Res.*, **19**, 6330.
Reddy,B.A., Freemont,P.S. and Etkin,L.D. (1992)*Trends Biochem. Sci.*, **17**, 344–345.
States,D.J., Haberkorn,R.A. and Ruben,D.J. (1982) *J. Magn. Reson.*, **48**, 286–292.
Searle,M.S. (1993) *Progr. Nucl. Magn. Spectr.*, **25**, 403–480.
Takahashi,M., Inaguma,Y., Hiai, H. and Hirose,F. (1988) *Mol. Cell. Biol.*, **8**, 1853–1856
de Thé,H.C., Lavau,A., Marchio,C., Chmornr,L., Degos and Dejean,A. (1991) *Cell*, **66**, 675–684.
Vaheri,A. and Pagano,J.S. (1965) *Virology*, **27**, 434–436.
Wagner,G., Braun,W., Havel,T.F., Schauman,T., Go,N. and Wüthrich,K.J. (1987) *Mol. Biol.*, **196**, 611–639.
Weis,K., Rambaus,S., Lavau,C., Jansen,J., Carvalho,T., Carmo-Fonseca,M., Lamond,A. and Dejean,A. (1994) *Cell*, **76**, 345–356.
Wüthrich,K. (1986) *NMR of Proteins and Nucleic Acids*. John Wiley and Sons, New York.
Xie,Z., Cai,W. and Schaffer,P.A. (1994) *J. Virol.*, **68**, 3027–3040.

*Received on November 21, 1994; revised on January 6, 1995*